

Development of a Near-Infrared Imaging System for Determination of Rice Moisture

Lian-Hsiung Lin,¹ Fu-Ming Lu,^{2,3} and Yung-Chiung Chang⁴

ABSTRACT

Cereal Chem. 83(5):498–504

The objective of this study was to develop a near-infrared (NIR) imaging system to determine rice moisture content. The NIR imaging system fitted with 15 band-pass filters (wavelengths of 870–1,014 nm) was used to capture the spectral image. In this work, calibration methods including multiple linear regression (MLR), partial least squares regression (PLSR), and artificial neural network (ANN) were used in both near-infrared spectrometry (NIRS) and the NIR imaging system to determine the moisture content of rice. Comprehensive performance comparison among MLR, PLSR, and ANN approaches has been conducted. To reduce repetition and redundancy in the input data and obtain a more accurate network, six significant wavelengths selected by the MLR model, which had high correlation with the moisture content of rice, were used as the input data of the ANN. The performance of the developed system was

evaluated through experimental tests for rice moisture content. This study adopted the coefficient of determination (r_{val}^2), the standard error of prediction (SEP), and the relative performance determinant (RPD) as the performance indices of the NIR imaging system with respect to the tests of rice moisture content. Utilizing these three models, the analysis results of r_{val}^2 , SEP, and RPD for the validation set were within 0.942–0.952, 0.435–0.479%, and 4.2–4.6, respectively. From experimental results, the performance of NIR imaging system was almost the same as that of NIRS. Using the developed NIR imaging system, all of the three different calibration methods (MLR, PLSR, and ANN) provided a high prediction capacity for the determination of moisture in rice samples. These results indicated that the NIR imaging system developed in this study can be used as a device for the measurement of rice moisture content.

Rice is the major staple food in Taiwan. Due to improvements in the living standards in Taiwan, superior rice quality is an important consumption criterion. The major physical properties that affect the taste and flavor of rice are moisture, protein, starch, and fat acidity content. Rice moisture content affects not only the milling yield and storability, but also the taste and flavor. The flavor of cooked rice is affected by physical properties including moisture content, cohesion, elasticity, and hardness. Among these, the moisture content of rice is the major factor influencing the flavor of cooked rice. Yamashita (1993) indicated that a moisture content of 15% gave a better rice flavor when other factors were similar. In general, low rice moisture content reduces the flavor of cooked rice. One of the reasons for this is that cracking occurred in rice before it was completely cooked. The starch leaked from the cracked rice during cooking, which increased the cohesion but decreased the flavor of the rice.

Techniques used to measure cereal moisture content can be classified as direct and indirect methods. The direct method involves removal of the water from cereal by oven heating. The moisture content ratio is then calculated from the weight loss. Although the traditional oven measurement (ASAE Standards, 1997) has high accuracy, this approach is time-consuming.

The indirect method measures the relationship between physical properties and the moisture content of the cereal. The moisture content was estimated based on cereal properties (density, resistance, dielectric property, etc.) (Grabe 1989). Near-infrared spectrometry (NIRS) has quickly evolved from a laboratory technique into a useful tool for a variety of qualitative and quantitative analysis tasks. Recent studies have demonstrated that NIRS could be used to estimate the chemical constituents, texture, and taste of

rice. Kawamura et al (1999) reported on the precision and accuracy of NIRS in determining the moisture content of rough rice. The instrument could scan 33 wavelengths of 825–1,075 nm. Li and Shaw (1997) developed the multiple linear regression (MLR) and partial least squares regression (PLSR) calibration models to determine the fat acidity of rough rice, and concluded that PLSR provided the optimal calibration model for fat acidity. Using the PLSR calibration model, samples with moisture contents of 12.7–16.7% obtained the coefficient of determination of 0.92. Delwiche et al (1995) reported on analysis of amylose and protein using a PLSR calibration model obtained from ground milled rice. The results were good but a large number of factors were required (18 for amylose and 16 for protein). Delwiche et al (1996) extended the application NIR reflectance spectra to whole grain milled rice. The obtained results were acceptable for both amylose and protein. Kawamura et al (1997) used MLR and PLSR analysis to assess the relationship of the taste evaluation to the spectra of whole grain milled rice. The best performance calibration model was obtained from original spectra of whole grain milled rice using MLR analysis. Sitakalin and Meullenet (2001) reported that spectral stress strain analysis was used in combination with PLSR and ANN to predict sensory texture attributes of cooked rice. They concluded that the ANN model was more significantly accurate than the PLSR.

Machine vision and image processing techniques provide a quick and objective means for measuring or evaluating the visual features of rice. Researchers' reports included using these techniques for the classification (Wan et al 2002), degree of milling measurement (Liu et al 1998; Yadav and Jinsal 2001), and stress crack detection (Wan et al 1997) of rice.

An NIR imaging system can capture images under many wavelength bands in the NIR region. Such imaging systems have been used for quality control and measurement in apples (Bellon et al 1992; Upchurch et al 1994) and in peaches and apricots (Miller and Delwiche 1990; Zwiiggelaar et al 1996). Sugiyama (1999) established an NIR imaging system to predict the sugar content of a cross-section of melon flesh. Furthermore, Tsuta et al (2002) applied the NIR spectroscopy theory to each pixel of the acquired images and developed a color distribution map of the sugar content of the melon surface. Ridgeway and Chambers (1998) used NIR imaging to detect insects inside wheat. Archibald et al (1998) developed an NIR system to analyze wheat protein

¹ Lecturer, Department of Biomechatronic Engineering, National Ilan University; PhD candidate, Department of Bio-Industrial Mechatronics Engineering, National Taiwan University, 136, Chou-Shan Rd., Taipei, 106, Taiwan.

² Professor, Department of Bio-Industrial Mechatronics Engineering, National Taiwan University, 136, Chou-Shan Rd., Taipei, 106, Taiwan.

³ Corresponding author. E-mail: lufuming@ntu.edu.tw

⁴ Assistant professor, Department of Horticulture, National Ilan University, 1, Sec. 1, Shen-Lung Rd., I-Lan, 260, Taiwan.

and color classification. Muramoto et al (2001) used NIR imaging to feature the moisture distribution on the surface of rough rice grains. Cogdill et al (2004) developed an NIR hyperspectral imaging technique that was able to calibrate and predict the moisture and protein contents of single maize kernels.

NIR spectroscopy technique is widely used for quality assessments of various crops. An NIR cooled charged couple device (CCD) camera captured spectral images in the NIR region such that the quantitative measurements become possible. NIR imaging techniques may not only be useful for quality evaluation but also for physiological analysis of cereal properties. In Taiwan, because of high humidity, it is important to control both temperature and moisture to preserve good quality of rice in the processing line. With the advancement of the high accuracy of NIR spectroscopy and the simple operation of the image processing system, the NIR imaging technique is very suitable to develop as a quick and non-destructive method for detecting rice qualities. Therefore, the objectives of this study were 1) to devise an NIR imaging system that can determine the moisture content of rice validly and 2) to investigate performance differences among the calibration curves using multiple linear regression (MLR), partial least squares regression (PLSR), and artificial neural network (ANN).

MATERIALS AND METHODS

Preparation of Rice Samples

The milled rice samples were collected from 40 different domestic markets, for a total of 15 cultivars. The tested samples included most of the popular medium- and long-grain rice cultivars consumed in Taiwan. The rice samples purchased from markets had moisture contents of 12–15%. To cover the different moisture levels of the rice, some samples were dried to reduce moisture content and, oppositely, some were rewetted to raise moisture content. There were 310 samples prepared for the experimental tests. A calibration set consisting of 232 samples was used to establish the MLR and PLSR models. The data measured from the same 232 samples were also used to build the ANN model, in which 155 samples were used as the training set and the remaining 77 samples were used as the monitoring set to cope with overfitting during training ANN. To compare the results of the three different calibration methods, the same validation set (the remaining 78 samples) was used.

Moisture Content Analysis

The standard value of sample moisture content was determined by oven drying. The rice sample with a weight of 25 g was dried at 105°C for 72 hr (Chen 2003). The moisture contents in this study are presented on a wet basis.

Near-Infrared Instrument

An NIR spectrometer (model 6500, Foss NIRSystems, Silver Spring, MD) was utilized to measure the moisture absorption bands. The Foss standard cup was filled with rice sample. The spectrometer scanned the sample in 2-nm steps between 400 and 2,500 nm and the spectra of reflection were measured. Scanning measurements for each sample were repeated three times.

Near-Infrared Imaging System

Figure 1 shows the configuration of the apparatus developed in this study to obtain the spectroscopic images. The system consists mainly of an NIR CCD camera (silicon type, C3077-78, Hamamatsu, Tokyo, Japan) with resolution of 780 (H) × 488 (V), which is coupled to a camera controller (C2741, Hamamatsu). A frame-grabber board (Meteor II, Matrox, Canada) was used to receive the video signal from the camera. A filter exchange device consisted of a filter adapter, a filter holder (DW01, Onset), and a stepper motor module that was combined with the CCD camera. The filters were installed in a filter holder. The filter exchange device was set up and its schematic diagram is shown in Fig. 2. The filter exchange device was controlled by a stepper motor to rotate automatically such that the NIR imaging system can effectively acquire multispectral images.

Wavelength ranges were selected carefully, taking both the NIR absorbing wavelength characteristics of rice and the suitable sensitivity range of CCD camera into consideration. In this study, 15 band-pass filters were used to extract spectra of the captured NIR image at 15 different central wavelengths. The characteristics of these filters including central wavelength, full-width at half-maximum band-pass, etc., are summarized in Table I. The detection wavelength range of the NIR imaging system was set at 870–1,014 nm. Four halogen bulbs (50W, 12V, OSRAM) illuminated the rice sample from four different positions to minimize the effects of shadows and direct reflection. The NIR CCD camera was located right above the sample. The distance between camera lens and the sample was 60 cm. The rice moisture inspection

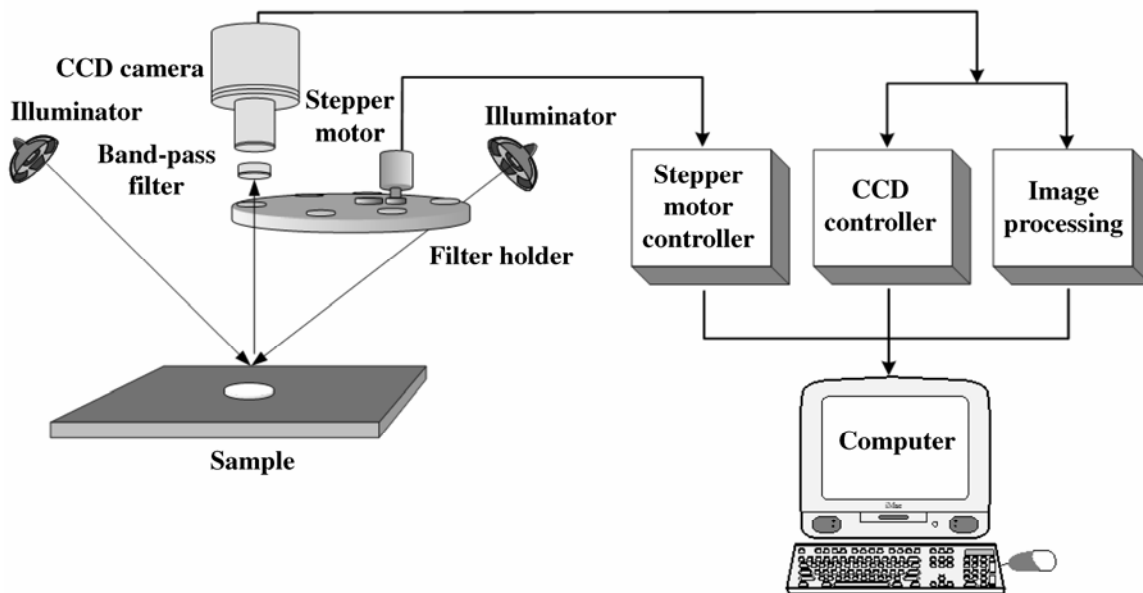


Fig. 1. Schematic diagram of developed NIR imaging system.

software for image processing and stepper motor control was developed in the Windows environment using a Borland C compiler.

Image Acquisition and Preprocessing

A rice sample (25 g) was evenly spread across a glass container 4 cm in diameter and 2 cm deep. The container and a reflectance standard (Ocean Optics WS-1, reflecting ratio > 98%, wavelengths 400–1,500 nm) were placed immediately below the camera. For every rice sample, there were 15 different wavelength images with 640 × 480 pixels captured by the CCD camera. To enhance the accuracy, only the 120 × 120 pixels located in the middle portion of each captured original image were used to calculate the average reflectance. The average reflectance obtained was used as the intensity of reflected light of the tested sample. To reduce the effects of different light source intensities, distances, and angles on the measured intensity of reflected light, the reflection of rice sample with respect to standard reflectance was corrected by Equation 1

$$R(\lambda) = \frac{I - I_D}{I_S - I_D} \quad (1)$$

where λ = wavelength, $R(\lambda)$ = reflection of the sample, I = intensity of reflected light of samples, I_S = intensity of reflected light of reflectance standard, and I_D = dark intensity.

The dark current (dark intensity offset) was due to the inherent structure of the CCD camera. I_D was the lowest reflectance measured by the CCD camera when the diaphragm of the CCD camera was closed and the light source turned off. The average reflectance at a specific wavelength was calculated by Equation 1 and then converted to absorbance spectrum $A(\lambda)$ by Equation 2

$$A(\lambda) = \log\left(\frac{1}{R(\lambda)}\right) \quad (2)$$

In our CCD system, both sample and reference standard were placed side-by-side below the camera and both images were captured at the same time. Therefore, both values of I and I_S were obtained simultaneously for every image extraction. If at any time, any sampling variable was changed, including intensity of reflected light, distance from light source to sample, etc., the reflectance standard spectrum was renewed.

Data Processing

The calibration models were established by using MLR, PLSR, and ANN methods, wherein the former two models are linear and the latter is nonlinear. The predictive capacities of the MLR,

PLSR, and ANN models were compared in terms of the coefficient of determination of calibration (r_{cal}^2), standard error of calibration (SEC), coefficient of determination of validation (r_{val}^2), standard error of prediction (SEP), and relative performance determinant (RPD), which is the ratio of standard deviation (SD) of the data in validation set to SEP ($RPD = SD/SEP$). For rating the reliability of these three models, Williams and Sobering (1993) suggested using the RPD value. According to their results, the prediction of calibration equations is reasonable when the RPD value ≥ 3 . The RPD rating was ranked as excellent (>10), very good (7–10), good (5–7), fair (3–5), or unsatisfactory (<3).

The MLR model was used to investigate the effects of the major absorption peak in the spectral data generated by NIRS on the prediction of rice moisture. The MLR calibration model between rice moisture content and the different absorption spectrum was established using the rice samples of the calibration set. Meanwhile, unsuitable wavelengths were eliminated employing stepwise regression analysis. After performing MLR analysis, the calibration equation with higher accuracy, i.e. with a smaller SEC and a larger r_{cal}^2 , can be obtained. Using the obtained calibration model to predict rice moisture contents of the validation set, a smaller SEP value and a higher r_{val}^2 value for variation between the predicted values and the standard measurements indicated that a better prediction model can be achieved.

The back-propagation (BP) ANN algorithm is widely used in chemometrics. The optimization criterion for the ANN network is to minimize the error of the training set or the monitoring set. Based on this approach, however, an overfitting model was frequently obtained (the minimum error of the validation set can not be achieved). To cope with this problem, the degree of approximation was employed (Liu et al 1996; Dou et al 2005). The definition of the optimization criterion for the ANN network is given in Equations 3 and 4

$$e_a = \left(\frac{n_t}{n}\right)e_t + \left(\frac{n_m}{n}\right)e_m + |e_t - e_m| \quad (3)$$

where e_a is the error of the approximation; e_t and e_m are the mean square errors of training set and monitoring set; n_t and n_m are the sample numbers of training set and monitoring set; n is the total number of samples, and

$$D_a = \frac{c}{e_a} \quad (4)$$

where D_a is the degree of approximation and c is a constant. The constant c was a scaling factor, which was utilized to adjust D_a to get a good chart. It is obvious that the smaller e_a or the larger D_a ,

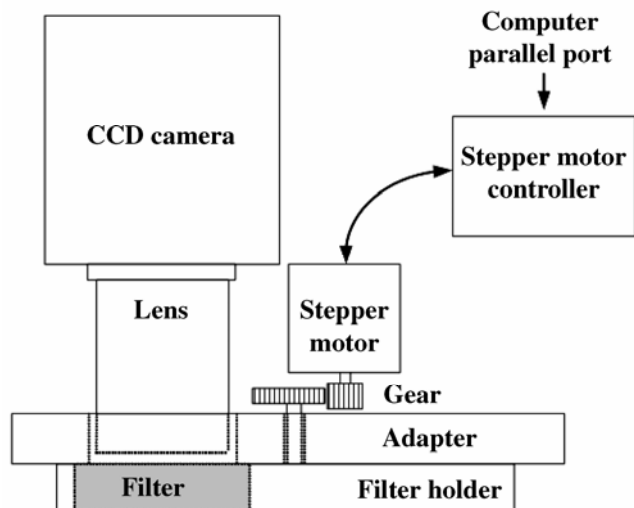


Fig. 2. Schematic diagram of the automatic filter exchange device.

TABLE I
Characteristics of Band-Pass Filters

Model	Central Wavelength (nm)		Full-Width at Half-Maximum Band-Pass (nm)
	Special Value	Measured Value	
870FS ϕ 25	870.0 \pm 3.0	871.43	10.11
880FS ϕ 25	880.0 \pm 3.0	881.56	10.22
890FS ϕ 25	890.0 \pm 3.0	891.11	10.66
900FS ϕ 25	900.0 \pm 3.0	901.06	10.52
910FS ϕ 25	910.0 \pm 3.0	912.98	10.88
920FS ϕ 25	920.0 \pm 3.0	922.15	10.95
930FS ϕ 25	930.0 \pm 3.0	932.62	11.51
940FS ϕ 25	940.0 \pm 3.0	940.15	8.63
950FS ϕ 25	950.0 \pm 3.0	952.89	8.78
960FS ϕ 25	960.0 \pm 3.0	962.16	8.59
970FS ϕ 25	970.0 \pm 3.0	971.76	8.72
980FS ϕ 25	980.0 \pm 3.0	981.02	8.98
990FS ϕ 25	990.0 \pm 3.0	990.62	8.95
1000FS ϕ 25	1,000.0 \pm 3.0	1,001.47	9.39
1014FS ϕ 25	1,014.0 \pm 3.0	1,015.29	9.34

the better the ANN model that can be obtained. The effects of both training and monitoring sets on D_a or e_a were considered in this work.

The MLR and PLSR regression analyses were performed using the Unscrambler software version 7.6 (Camo A/S, Trondheim, Norway). The algorithms of the ANN were developed by using the Neural Network Toolbox of MATLAB 6.5 (The MathWorks, Natick, MA).

RESULTS AND DISCUSSION

Table II shows the moisture analyses results of the 310 samples that were measured by oven method. The moisture content of rice was 9.64–17.27%. The average and standard deviation were 13.76–13.77% and 1.96–2.00%, respectively.

Determining the Moisture Content of Rice by MLR

To determine which band of the wavelength has high correlation with moisture content of rice, the data measured using the NIRS and the NIR imaging system with a spectral range of 870–1,014 nm were analyzed and compared with each other. The selected wavelength range covers the spectral range of the CCD camera used in developing an NIR imaging system.

Table III summarized the evaluation results of moisture content analysis employing the MLR model. For example, the results predicted by NIRS were $r_{cal}^2 = 0.975$, SEC = 0.329%, and RPD = 5.5 when the wavelengths of 960, 930, and 980 nm were selected. The calibration equation that included six wavelengths of 960, 930, 980, 1,000, 940, and 1,014 nm gave $r_{cal}^2 = 0.987$, SEC = 0.240%, and RPD = 8.1. The analysis results for NIRS were listed Table III for comparison with those for the NIR imaging system.

The same MLR analysis procedure for the NIR imaging system case was then conducted (Table III). The analysis results for single wavelength 960 nm measurements produced $r_{val}^2 = 0.448$ and SEP = 1.462%. The values of r_{val}^2 , SEP, and RPD were respectively 0.911, 0.596%, and 3.4 when three wavelengths of

960, 930, and 980 nm were adopted. When six wavelengths of 960, 930, 980, 1,000, 900, and 940 nm were selected, the $r_{val}^2 = 0.942$, SEP = 0.479%, and RPD = 4.2. When the number of selected wavelengths was greater than six, SEC, RPD, and r_{val}^2 decreased but SEP increased. This caused an overfitting problem because factors other than rice moisture might be included in the captured spectrum information. Therefore, the MLR prediction model for rice moisture content using the NIR imaging system achieved its best performance when six wavelengths were adopted. These selected wavelengths appeared near the typical absorption bands of water (Williams and Norris 1990). The MLR model was expressed as Moisture (%) = 11.10 + 433.76 $\log(1/R_{960}) - 320.07 \log(1/R_{930}) - 91.89 \log(1/R_{980}) - 91.57 \log(1/R_{1,000}) + 73.56 \log(1/R_{900}) + 22.89 \log(1/R_{940})$.

Determining the Moisture Content of Rice by PLSR

The PLSR method was used to evaluate the prediction capability of the different wavelength ranges. The calibration and prediction results employing PLSR analysis are shown in Table IV. The predictions of NIRS employing PLSR within the wavelength range of 930–1,014 nm produced the best results. This gave $r_{val}^2 = 0.987$, SEP = 0.245%, and RPD = 8.2. Moreover, the six wavelengths employed in the calibration equation of the MLR analysis fell within the range of 930–1,014 nm in the PLSR model. The larger wavelength range of 1,100–2,500 nm could offer more information, but it would include unwanted data such that the SEP increased to 0.464% as compared with 0.245% for the 930–1,014 nm range. This illustrates that a wider wavelength range does not necessarily result in better prediction results. Therefore, it is important to choose the suitable spectrum information to give the best prediction. The prediction results for the NIR imaging system employing the PLSR analysis model for the wavelength range of 870–1,014 nm obtained $r_{val}^2 = 0.952$, SEP = 0.435%, and a RPD = 4.6. When these results are compared with those of the NIRS, the developed NIR imaging system can provide a satisfactory prediction capability.

TABLE II
Statistical Analysis for Moisture Content (% wb) of Samples Using MLR, PLSR, and ANN

	MLR, PLSR		ANN		
	Calibration Set	Validation Set	Training Set	Monitoring Set	Validation Set
Mean ± SD	13.76 ± 1.96	13.76 ± 2.00	13.76 ± 1.97	13.77 ± 1.97	13.76 ± 2.00
Minimum	9.78	9.64	9.78	9.84	9.64
Maximum	17.27	17.17	17.27	17.06	17.17
Sample size	232	78	155	77	78

TABLE III
Performance Comparison^a Between NIRS and NIR Imaging System Using Multiple Linear Regression (MLR) Model

Instrumentation and Selected Wavelengths (nm)	r_{cal}^2	SEC	r_{val}^2	SEP	RPD
NIRS					
960	0.546	1.423	0.445	1.538	1.3
960+1,014	0.900	0.697	0.880	0.723	2.8
960+930+980	0.975	0.329	0.970	0.362	5.5
960+930+980+1,000	0.979	0.303	0.972	0.351	5.7
960+930+980+1,000+940	0.985	0.252	0.973	0.347	5.8
960+930+980+1,000+940+1,014	0.987	0.240	0.986	0.247	8.1
NIR Imaging					
960	0.457	1.464	0.448	1.462	1.4
960+1,014	0.753	0.978	0.733	1.026	1.9
960+930+980	0.918	0.565	0.911	0.596	3.4
960+930+980+1,000	0.928	0.528	0.918	0.574	3.5
960+930+980+1,000+900	0.943	0.469	0.933	0.514	3.9
960+930+980+1,000+900+940	0.948	0.448	0.942	0.479	4.2
960+930+980+1,000+900+940+990	0.950	0.439	0.939	0.492	4.1
960+930+980+1,000+900+940+990+970	0.952	0.435	0.934	0.513	3.9

^a Coefficient of determination of calibration (r_{cal}^2); standard error of calibration (SEC); coefficient of determination of validation (r_{val}^2); standard error of prediction (SEP); relative performance determinant (RPD), ratio of standard deviation (SD) of the data in validation set to SEP (RPD = SD/SEP).

TABLE IV
Performance Comparison^a Between NIRS and NIR Imaging System Using Partial Least Square Regression (PLSR) Model

Instrumentation and Wavelengths Range (nm)	No. of Factors	r_{cal}^2	SEC	r_{val}^2	SEP	RPD
NIRS						
1,100–2,500	4	0.962	0.406	0.950	0.464	4.3
870–1,014	4	0.970	0.360	0.963	0.400	5.0
930–1,014	5	0.988	0.239	0.987	0.245	8.2
NIR Imaging						
870–1,014	8	0.960	0.396	0.952	0.435	4.6

^a Coefficient of determination of calibration (r_{cal}^2); standard error of calibration (SEC); coefficient of determination of validation (r_{val}^2); standard error of prediction (SEP); relative performance determinant (RPD), ratio of standard deviation (SD) of the data in validation set to SEP (RPD = SD/SEP).

TABLE V
Performance Comparison^a Between NIRS and NIR Imaging System Using Artificial Neural Network (ANN) Model

Instrumentation	Components ^b	Training Set			Monitoring Set		Validation Set		
		r_{cal}^2	SEC	MSE	r^2	MSE	r_{val}^2	SEP	RPD
NIRS	6,3,1	0.990	0.211	0.008	0.986	0.015	0.984	0.259	7.7
NIR Imaging	6,5,1	0.974	0.318	0.025	0.953	0.050	0.952	0.435	4.6

^a Coefficient of determination of training (r_{cal}^2); standard error of training (SEC); mean square error (MSE); coefficient of determination of monitoring (r^2); coefficient of determination of validation (r_{val}^2); standard error of prediction (SEP); relative performance determinant (RPD) = ratio of standard deviation (SD) of the data in validation set to SEP (RPD = SD/SEP).

^b Net architecture neurons in the input, hidden, and output layers (i, h, o) respectively.

Determining the Moisture Content of Rice by ANN

In this work, a feedforward ANN was utilized to estimate the moisture content of rice. The proposed ANN consists of three layers: input, hidden layer, and output. Each layer contains several neurons and the activation functions utilized in the hidden neurons and the output neurons were sigmoid function and linear function, respectively. The usual way of describing the architecture of a network is by using the notation (i, h, o), where i is the number of neurons in the input layer; h is the number of neurons in the hidden layer; and o is the number of neurons in the output layer. The number of neurons in the input and hidden layers should be optimized. The issue of setting up a proper amount of neurons in an ANN is still an open problem at this time. Reducing the redundancy on the input data to a network reduces training time and produces a more accurate network. Therefore, the MLR is used to reduce the large amount of data. MLR filtered the data and then the selected significant wavelengths were fed into the input of the ANN. Because only the moisture content of rice was to be predicted, the output layer contained one neuron.

The number of hidden neurons affects the performance of the proposed ANN classifier. Figure 3 shows the effects of the number of hidden neurons on the error indices e_t , e_m , and D_a for the developed NIR imaging system. The number of neurons of the hidden layer was sequentially increased from 1 to 10 to determine the optimal amount of neurons needed by the proposed ANN. In Fig. 3, curves a and b, which represented the mean square error of training set e_t and monitoring set e_m , respectively, varied randomly. Hence, it was difficult to determine the optimum number of hidden nodes. Curve c in Fig. 3 is the degree of approximation curve. From curve c, it is clear that the maximum value of D_a was achieved when the five hidden neurons were used. Thus, the optimal number of hidden neurons was five according to the criterion of the largest degree of approximation. Using the same approach, an optimal ANN model of NIRS was also established.

Table V shows the prediction results obtained in the ANN models of both the NIRS and the NIR imaging system. ANN was trained using both the training sets (155 samples) and the monitoring sets (77 samples). The validation sets (78 samples) of MLR and PLSR were used as the validation set of ANN.

The ANN model set up by NIRS gave a high prediction capability ($r_{\text{val}}^2 = 0.984$). The ANN model based on the developed NIR imaging system also provided a satisfactory prediction result with $r_{\text{val}}^2 = 0.952$. An inspection of the prediction results sum-

marized in Table V clearly demonstrates that ANN model provides similar reliability to the PLSR model. Because the validation set was not used in training networks, its standard error (SEP) was higher than that of training set (SEC) and coefficient of determination (r_{val}^2) was lower than that of training set (r_{cal}^2). Also, the prediction results for the validation set were similar to those of the monitoring set. This means that the ANN model is quite suitable for predicting the moisture content of rice. Moreover, the method using the maximum value of the degree of approximation corresponding to the minimum value of the error of prediction in the validation set is feasible.

Using MLR, PLSR, and ANN analyses, the regression relationships of moisture content between the reference data from the oven method and the prediction data from the NIR imaging system are shown in Fig. 4. In the PLSR and ANN models, both the regression curves had almost the same high value of $r_{\text{val}}^2 = 0.952$. Using MLR model, $r_{\text{val}}^2 = 0.942$. In this work, all three calibration methods (MLR, PLSR, and ANN) provided a high prediction capacity for the determination of moisture in rice samples using the developed NIR imaging system.

An examination of Fig. 4 clearly indicates that all the models achieved a good relationship with rice moisture content. The MLR model needed only six wavelengths to obtain a calibration equation. The PLSR model calculated every wavelength in the whole wavelength range, so capturing the effective wavelength range was a very important step. Comparing the MLR and PLSR models, the PLSR model had a better prediction capacity, which was shown by the higher RPD = 4.6. However, it needed more spectrum information (15 wavelengths) in the wavelength range of 870–1,014 nm than MLR (six wavelengths). In the ANN model, the net input using the six wavelengths spectrum selected by MLR had the advantages of being quick, simple, and provided a high detection accuracy (RPD = 4.6) during application to a real situation. Therefore, this approach should be adopted for the NIR imaging system when it is set up commercially.

CONCLUSIONS

An NIR imaging system to determine rice moisture content was developed. The related image processing programs were also developed and equipped into the system. The developed NIR imaging system can automatically and effectively acquire multi-spectral images and obtain absorbance values of the spectroscopic

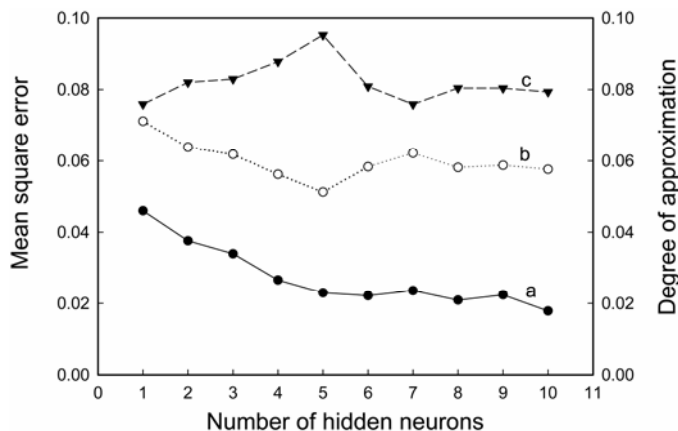


Fig. 3. Effect of hidden neurons for (a) mean square error of training set, (b) mean square error of monitoring set, (c) degree of approximation.

images using the developed image processing programs. Many experimental tests were conducted to verify the performance of the developed NIR imaging system. For comparison, same experimental procedures also had been performed using commercial NIRS.

The effects of MLR, PLSR, and ANN analyses models of the NIR imaging absorption spectrum on the detection accuracy and reliability of rice moisture content were investigated in detail in this study. For the MLR model, six significant wavelengths of 960, 930, 980, 1,000, 900, and 940 nm were selected to obtain calibration equation for rice moisture content with high prediction capability. Employing PLSR analysis model, a better prediction than the MLR approach was achieved. However, it needed more input wavelengths when the PLSR approach was applied. Results of the ANN model had performance similar to that of PLSR model. These tests demonstrated that the NIR imaging system using MLR, PLSR, and ANN models can provide comparable detection capability for rice moisture.

The experimental tests indicated that the developed NIR imaging system might have the potential to achieve performance in moisture content evaluation similar to commercial NIRS. This verified that the developed NIR imaging system can be used to accurately determine moisture content of rice. Therefore, the developed NIR imaging system may serve as an alternate for a quick and nondestructive detection system of rice moisture content. In a future study, the system will be applied to the analyses of other important rice content parameters.

LITERATURE CITED

Archibald, D. D., Thai, C. N., and Dowell, F. E. 1998. Development of short-wavelength near-infrared spectral imaging system for grain color classification. *Proc. SPIE* 3543:189-198.

ASAE. 1997. Oven temperature and heating period for moisture content determination. Standard S352.2. The Association: St. Joseph, MI.

Bellon, V., Rabatel, G., and Guizard, C. 1992. Automatic sorting of fruit: Sensors for the future. *Food Control* 1:49-54.

Chen, C. 2003. Evaluation of air oven moisture content determination methods for rough rice. *Biosys. Eng.* 86:447-457.

Cogdill, R. P., Hurburgh, C. R., and Rippke, G. R. 2004. Single-kernel maize analysis by near-infrared hyperspectral imaging. *Trans. ASAE* 47:311-320.

Delwiche, S. R., Bean, M. M., Miller, R. E., Webb, B. D., and Williams, P. C. 1995. Apparent amylose content of milled rice by near-infrared reflectance spectrophotometry. *Cereal Chem.* 72:182-187.

Delwiche, S. R., McKenzie, K. S., and Webb, B. D. 1996. Quality characteristics in rice by near-infrared reflectance analysis of whole-grain milled samples. *Cereal Chem.* 73:257-263.

Dou, Y., Sun, Y., Ren, Y. Q., and Ren, Y. L. 2005. Artificial neural network for simultaneous determination of two components of compound paracetamol and diphenhydramine hydrochloride powder on NIR spec-

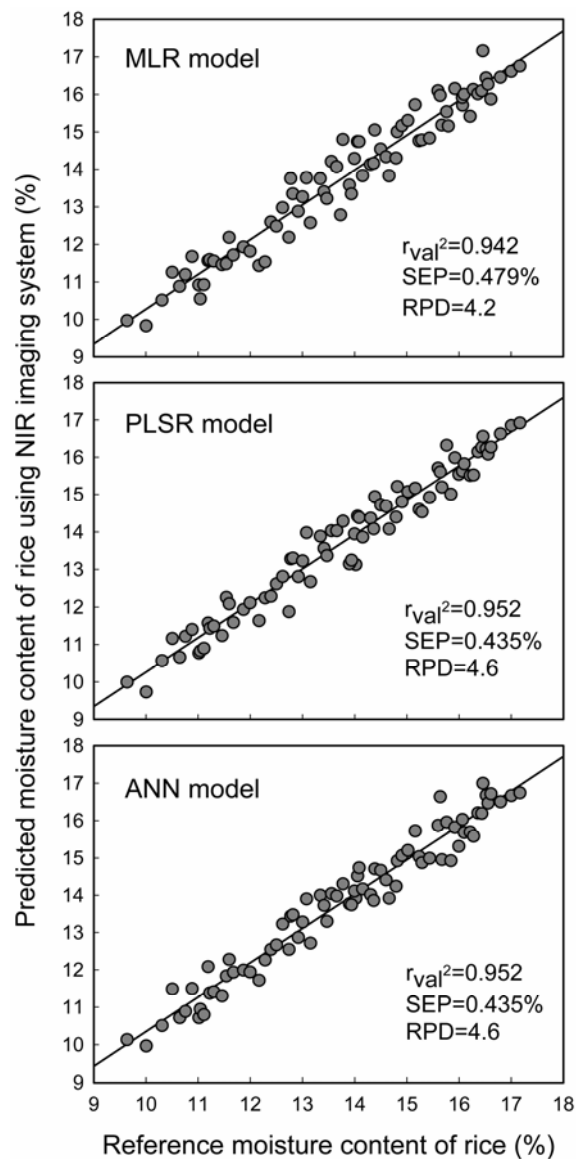


Fig. 4. Performance validation of NIR imaging system using three different calibration models.

troscopy. *Anal. Chim. Acta* 528:55-61.

Grabe, D. F. 1989. Measurement of seed moisture. In: *Seed Moisture*. CSSA Special Publication No.14. CSC: Madison, WI.

Kawamura, S., Natsuga, M., and Itoh, K. 1997. Visual and near-infrared reflectance spectroscopy for rice taste evaluation. *Trans. ASAE* 40:1755-1759.

Kawamura, S., Natsuga, M., and Itoh, K. 1999. Determination of undried rough rice constituent content using near-infrared transmission spectroscopy. *Trans. ASAE* 42:813-818.

Li, W. S., and Shaw, J. T. 1997. Determining the fat acidity of rough rice by near-infrared reflectance spectroscopy. *Cereal Chem.* 74:556-560.

Liu, P., Liang, Y., Zhang, L., and Yu, R. 1996. Artificial neural networks applied in the analysis of chemical data (1)—Approximation for over-fitting. *J. Chin. Chem.* 17:861-865.

Liu, W., Tao, Y., Siebenmorgen, T. J., and Chen, H. 1998. Digital image analysis method for rapid measurement of rice degree of milling. *Cereal Chem.* 75:380-385.

Miller, B. K., and Delwiche, M. J. 1990. Spectral analysis of peach surface defects. ASAE Paper No. 906040. The Association: St. Joseph, MI.

Muramoto, A., Kato, K., and Morio, Y. 2001. Moisture distribution image of grain layer surface using multi-wavelength near 970 nm. Pages 229-232 in: *3rd IFAC/CIGR Workshop on Control Applications in Post-Harvest and Processing Technology*. Pergamon: Oxford, UK.

Ridgeway, C., and Chambers, J. 1998. Detection of insects inside wheat kernels by NIR imaging. *J. Near-Infrared Spectrosc.* 6:115-119.

- Sitakalin, C., and Meullenet, J. F. C. 2001. Prediction of cooked rice texture using an extrusion test in combination with partial least squares regression and artificial neural networks. *Cereal Chem.* 78:391-394.
- Sugiyama, J. 1999. Visualization of sugar content in the flesh of a melon by near-infrared imaging. *J. Agric. Food Chem.* 47:2715-2718.
- Tsuta, M., Sugiyama, J., and Sagara, Y. 2002. Near-infrared imaging spectroscopy based on sugar absorption band for melons. *J. Agric. Food Chem.* 50:48-52.
- Upchurch, B. L., Throop, J. A., and Aneshansley, D. J. 1994. Influence of time, bruise type, and severity on near-infrared reflectance from apple surface for automatic bruise detection. *Trans. ASAE* 37:1571-1575.
- Wan, Y. N., Lin, C. M., Liao, C. H., and Chou J. J. 1997. Image analysis and application of reflection of cracked rice. *J. Agric. Machin.* 6(3):89-99.
- Wan, Y. N., Lin, C. M., and Chiou J. F. 2002. Rice quality classification using an automatic grain quality inspection system. *Trans. ASAE* 45:379-387.
- Williams, P. C., and Norris, K. H. 1990. Qualitative application of near-infrared reflectance spectroscopy. In: *Near-Infrared Technology in the Agricultural and Food Industries*. P. C. Williams and K. H. Norris, eds. AACC International: St. Paul, MN.
- Williams, P. C., and Sobering, D. C. 1993. Comparison of commercial near infrared transmittance and reflectance instruments for analysis of whole grain and seeds. *J. Near Infrared Spectrosc.* 1:25-32.
- Yadav, B. K., and Jindal, V. K. 2001. Monitoring milling quality of rice by image analysis. *Computers Electronics Agric.* 33:19-33.
- Yamashita, R. 1993. *New technology in grain postharvesting*. Farm Machinery Indus. Res. Corp. Tokyo: Japan.
- Zwiggelaar, R., Yang, Q., Garcia, P., and Bull, C. R. 1996. Use of spectral information and machine vision for bruise detection on peaches and apricots. *J. Agric. Eng. Res.* 63:323-331.

[Received August 1, 2005. Accepted April 26, 2006.]